Oxidation of Acetic Acid Solutions in a Trickle-Bed Reactor

Rates of oxidation of dilute, aqueous solutions of acetic acid were measured at 252° to 286°C and 67 atm in liquid full and trickle-bed reactors packed with ferric oxide catalyst particles. Predicted global rates and conversions indicated that localized vaporization and liquid channeling could affect trickle-bed performance.

JANEZ LEVEC
and
J. M. SMITH
University of California
Davis, California

SCOPE

Oxidation of dilute aqueous solutions of organic pollutants by using solid catalysts offers an alternate process to biological oxidation as a means of purifying liquid water. Hamilton et al. (1969) described such a process using a magnesia catalyst at 100°C. Sadana and Katzer (1974) have reported conversions of phenol to carbon dioxide of as high as 90% using a copper oxide catalyst at 145°C and 17 atm pressure. Not enough oxygen can be dissolved in water to give high conversions and still operate the reactor liquid full. Therefore, a gas-liquid-solid system, such as a trickle-bed reactor where gas (air or oxygen) and liquid flow concurrently downwards through the catalyst bed, is needed. Alternately, a slurry reactor with gas bubbling through the slurry could be used. In these three-phase systems, finite mass transfer rates between gas and liquid as well as between liquid and solid can affect reactor performance. Also, inefficient contact areas between the phases, due, for example, to channeling, can influence results. Goto and Smith (1975*a*, *b*) studied the oxidation of formic acid in water in a trickle-bed reactor using a CuO·ZnO catalyst operated at 40 atm and 200° to 240°C. Elevated pressure was necessary to maintain water in the liquid phase. Based on a model which accounted for gas-to-liquid, liquid-to-particle, and intraparticle diffusion, they were able to predict observed behavior reasonably well from intrinsic kinetics and effectiveness factors previously established (Baldi et al., 1974) from data obtained in liquid full operation. Formic acid is easily oxidized. Hence, relatively low temperatures could be used so that the vapor pressure of the liquid was low. Because the intrinsic rate was large, short catalyst beds and high liquid rates were satisfactory, perhaps avoiding uncertainties due to inefficient contacting between phases. Another published study in trickle beds, which accounts for mass transfer effects, is that of Hartman and Coughlin (1972) on the oxidation of sulfur dioxide in a bed of activated carbon. These authors also found that liquid phase and intraparticle diffusion adversely affected the conversion to sulfur trioxide. Investigations such as these which attempt to account for all mass transport factors are rare. In a useful review, Satterfield (1975) has summarized current design concepts and indicated the need for additional kinetics and transport research. The effect of efficiency of liquid particle contacting on reactor performance has been investigated by Satterfield and May (1972) and by Sedricks and Kenney (1973).

As a further study of trickle-bed performance, this paper reports results for the oxidation of acetic acid in water. Acetic acid is a rather refractory pollutant requiring relatively high temperatures, low liquid rates, and deep catalyst beds for high conversion to carbon dioxide. An iron oxide catalyst was employed in a 2.54 cm I.D. reactor operated at 252° to 286°C and 67 and 72.5 atm. Three types of experimental data were obtained: intrinsic kinetics from liquid full (no gas phase) operation at low conversions; global reaction rates from trickle-bed operation, again at low conversions; and high conversion, trickle-bed results. These data then were compared with predictions of global rates and integral conversions by using available mass transfer information. The objective is to obtain a better understanding of the behavior of trickle-bed reactors. No published information was uncovered for the kinetics of oxidation of aqueous solutions of acetic acid with oxygen. Hence, the liquid full results also are useful from a kinetics viewpoint.

CONCLUSIONS AND SIGNIFICANCE

The kinetics data for different catalyst particle sizes and flow rates in the liquid full reactor showed no effects of intraparticle diffusion or liquid-to-particle mass transfer. These results showed that the rate was one-half order in oxygen and decreased from first order to nearly zero order as the concentration of acetic acid increased. The activation energy was 21 kcal/mole in comparison with 37 kcal/mole found by Baldi, et al. (1974) for the oxidation of aqueous solutions of formic acid. Measurable concentrations of intermediates, such as acetaldehyde or formic acid, were not found by chromatographic analysis.

The trickle-bed data at the differential-reactor level gave global rates that increased more slowly with temperature than intrinsic rates due not only to gas-liquid-particle transport resistances but also to the large increase in vapor pressure of water with temperature in the 250° to 280°C range. Since the reactor was operated at constant total pressure, an increase in water vapor pressure caused a decrease in oxygen partial pressure which had an adverse effect on the rate. To predict global rates it was assumed that oxygen had to be transferred through separate gas-liquid and liquid-particle interfaces before active catalyst was reached. This model gave rates that agreed reasonably well with the experimental values at low temperatures, but experimental rates were much larger at high temperatures. This could be due to local vaporization of part of the water on the catalyst surface, thus reducing mass transfer resistances.

Measured conversions to carbon dioxide in deeper catalyst beds were less than those predicted from intrinsic

Janez Levec is on leave from the University of Ljubljana, Yugoslavia.

kinetics and reactor models at low liquid rates, but agreement was good at high rates. The deviation at low liquid flows occurred despite the fact that the predicted global rates were greater than experimental values. A possible explanation for these opposite effects is increased channeling of the liquid with decreasing liquid rates in the relatively deep catalyst beds.

Comparisons with similar results for the more easily oxidizable formic acid (Goto and Smith, 1975*b*) suggests that additional research is needed on trickle-bed reactor performance. The reactivity change between formic and acetic acid leads to large differences in operating conditions, particularly catalyst bed depths, temperature, and liquid flow rates. These differences may affect the nature of mass transport processes at the global rate level and affect liquid and gas distribution through the reactor. Particularly desirable would be studies of the effect of volatility of the solvent, and potential vaporization on mass transfer resistances between vapor-liquid-particle surface, and studies of the influence of liquid flow rate and catalyst bed depth on liquid channeling.

The oxidation of dilute aqueous solutions of acetic acid apparently has not been studied heretofore. However, there have been gas phase investigations (Gorshkov et al., 1968; Margolis, 1971) of the final stages of hydrocarbon oxidations. Based upon data for acetaldehyde, it was proposed that oxidation occurs via intermediates of formaldehyde, formic acid, and carbon monoxide. These results are helpful in formulating a scheme of reactions for our aqueous solution studies, although the only measurable product formed was carbon dioxide. Our intrinsic kinetics experiments were carried out in the same apparatus that was used for the subsequent trickle-bed data except that the reactor was smaller in diameter and operated upflow, liquid full. Data were taken over a range of flow rates and for widely different particle sizes in order to test for liquid-particle surface mass transfer resistance and intraparticle diffusion in the liquid filled pores. Particles of the same catalyst batch were used for both intrinsic kinetics and trickle-bed measurements.

In the trickle-bed work, the behavior of the liquid distributor was tested by visual observation, before and after the runs, by using a glass tube operated at atmospheric pressure. While liquid distribution appeared to be uniform under atmospheric conditions, observation during a high pressure run could not be made because a steel reactor had to be used. Reactor pressure and flow rates could be maintained constant without difficulty by using an automatic control valve and controller, as described in the experimental section.

EXPERIMENTAL

Apparatus

Figure 1 is a schematic drawing of the apparatus for trickle-bed operation. The downflow reactor [12] was 2.54 cm I.D. and 30 cm long.

For intrinsic kinetics runs, this reactor was replaced by another consisting of a 25 cm length of 0.93 cm I.D. stainless steel tubing. Only liquid with predissolved oxygen was fed upflow to this reactor. The remainder of the apparatus was the same as for trickle-bed operation except the phase separators [15] were not used.

Liquid feed of the known acetic acid concentration was prepared from distilled water and reagent grade acid and maintained saturated with oxygen by bubbling air (oxygen-

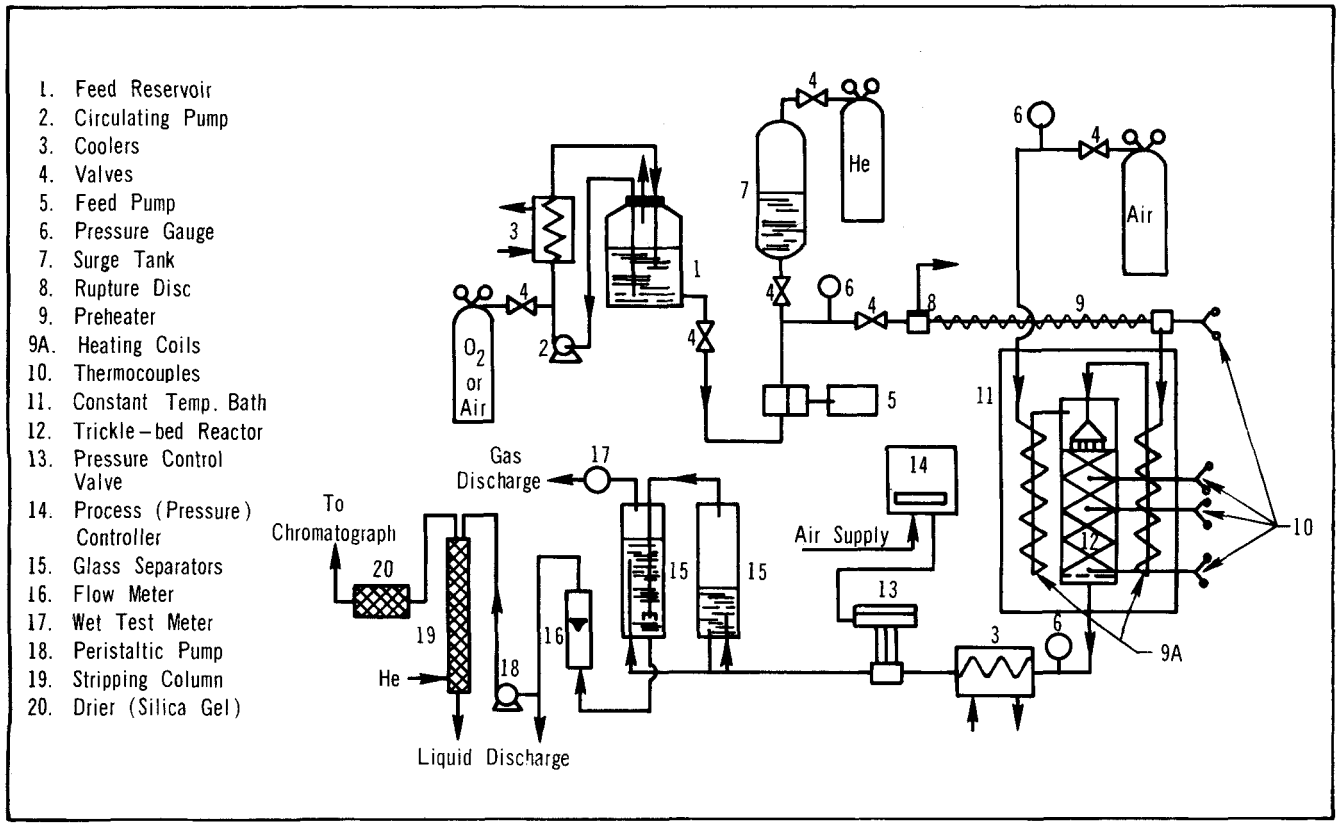

Fig. 1. Diagram of trickle-bed apparatus.

nitrogen mixtures for intrinsic kinetics runs) through the feed reservoir [1]. A cooler [3] and circulating pump [2] were employed to maintain constant temperature in the reservoir. This liquid was fed to the reactor by diaphragm metering pump [5]. Small pressure fluctuations in the pump discharge were dampened with surge tank [7]. The feed was heated to reaction temperature in an electric preheater [9] and in a coil [9A] immersed in the constant-temperature bath [11] containing the reactor. The air for trickle-bed operation was heated in a similar coil [9A] and also fed to the top of the reactor [12].

The catalyst bed for intrinsic-kinetics runs was packed with approximately equal volumes of uniformly distributed glass beads (70 mesh) and catalyst particles. For trickle-bed operation, the catalyst was not diluted with glass beads. Glass beads were also placed before and after the catalyst to reduce channeling. Properties of the catalyst bed and reactor operating conditions are listed in Table 1. Since the operating pressure was 67.5 atm. and the oxygen was dissolved in the liquid feed at atmospheric pressure, there was no gas phase present in the reactor.

For trickle-bed operation, the liquid was introduced downwards through the distributor (see Figure 1) which consisted of five capillary tubes placed so that the flux of liquid was approximately uniform over the cross-sectional area. The capillary tubes were 0.5 cm long and 0.1 cm I.D. These dimensions were such that the flow of liquid was essentially the same from each tube. To reduce end effects, the exits of the five capillary tubes were positioned 0.2 cm above the catalyst bed.

Temperatures were measured with iron-constantan thermocouples [10] placed at three axial locations (Figure 1) and in the feed line. For intrinsic-kinetics data thermocouples were placed at the entrance and exit of the bed. No temperature rise due to reaction was observed in any of the runs. This was expected, since the acetic acid concentration never exceeded 500 p.p.m.

The effluent from the reactor flowed through cooler [3] and then through pressure control valve [13] (Badger Meter Co., Inc. Type 785, ¼ in.). The latter was activated by air controller [14] Taylor Instrument Co., 440R, 0 to 1 000 lb/sq in.) which served to maintain constant pressure in the reactor. The low pressure effluent from the valve was fed to separators [15]. The gas from the first separator was introduced to the bottom of the liquid in the second separator through a dispersion tube. In this way, the gas and liquid leaving the second separator were at near equilibrium compositions. The approach to gas-liquid absorption equilibrium in such separators was found by Goto and Smith (1975*b*) to be excellent, even when one separator was used. With this arrangement, the total oxygen and carbon dioxide content of the reactor effluent could be established by analyzing only the liquid from the second separator and by using equilibrium compositions for the gas stream. The flow rates of liquid and gas were measured in rotometer [16] and wet test meter [17], respectively. Part of the liquid stream was analyzed by stripping it with helium in packed column [19] and by analyzing the stripped gas in a chromatograph.

Analysis

The stripping column had been tested for stripping efficiency by Baldi et al. (1974) and was operated at flow rates such that essentially all of the carbon dioxide and oxygen were removed from the liquid. The oxygen in the helium stream from the stripping column was determined in the chromatograph by using a 6 m length, 0.63 cm O.D. column packed with 5A molecular sieve particles (20 to 60 mesh). Carbon dioxide was determined in a 3 m, 0 63 cm O.D. column packed with 80 to 100 mesh Poropak Q. Both columns were operated at 100°C.

No acetic acid nor carbon monoxide was detected in the gas stream from the stripping column. For material balance calculations, the carbon content of the liquid from the stripping column was analyzed periodically in a Beckman (Model 915) Total Organic Carbon (TOC) Analyzer. To check for intermediates, the reactor effluent was also analyzed in a gas chromatograph by using a column specially designed to identify organic acids and aldehydes. With this column, consisting of a 3 m length of glass tubing (0.63 cm O.D.) packed with 5% FFAP (free fatty acid) on Chromosorb T (40 to 60 mesh) and operated at 130° C with FID detector at 140° C, no formic acid or formaldehyde was detected.

TABLE 1. OPERATING CONDITIONS

Kinetic runs (Liquid full reactor)	
1. Mass of catalyst, g	3.0(d_p = 0.0386) and 3.6(d_p = 0.238)
2. Catalyst particle size, d_p, cm	0.0384* and 0.238**
3. Liquid flow rate at 25°C, 1 atm, cm³/s	0.48, 0.65, 0.81
4. Temperature, °C	252, 260, 269, 277, 286
5. Pressure, atm	67, 72.5 (at 286°C)
6. Feed concentrations:	
Oxygen, (mole/cm³) × 10⁷	2.5, 4.8, 7.3, 10.5
Acetic acid, (mole/cm³) × 10⁷	8.3, 17.0, 26.5, 33.3, 45.8, 70.8
Trickle-bed runs	
1. Mass of catalyst, g	
Differential reactor	13(d_p = 0.0541) and 15(d_p = 0.238)
Integral reactor	107(d_p = 0.238)
2. Catalyst bed length, cm	
Differential reactor	2.2(d_p = 0.0541) and 2.4(d_p = 0.238)
Integral reactor	17.5(d_p = 0.238)
3. Catalyst particle size, d_p, cm	0.0541† and 0.238**
4. Liquid flow rate (at 25°C, 1 atm), cm³/s	0.38, 0.52, 0.66, 0.95, 1.32
5. Gas flow rate (at 25°C, 1 atm), cm³/s	1.6, 3.5, 5.9
6. Temperature, °C	252, 260, 269, 277, 286
7. Pressure, atm	67, 72.5 (at 286°C)
8. Liquid feed concentration	
Oxygen, mole/cm³	2.40 × 10⁻⁷
Acetic acid, mole/cm³	33.3 × 10⁻⁷

* 35 to 42 mesh.
† 28 to 32 mesh.
** 1/8 × 1/16 in. pellets.

Catalyst Properties and Pretreatment

In preliminary experiments with liquid full reactor operation, the activity of several catalysts was tested by measuring the rate of production of carbon dioxide. The tests were carried out at 240° C and 40 atm pressure by using identical weights of 35 to 42 mesh catalyst particles and a liquid feed containing 200 mg/l of acetic acid and 35 mg/l of oxygen (corresponding to saturation with pure oxygen at 1 atm). Untreated copper-chromite catalysts (G-13 and G-T531 from Chemetron Corporation) were found to be the most active. However, both gave yellow colored liquid effluents, and activity dropped sharply after a few hours operation. After a pretreatment consisting of bubbling oxygen through a suspension of the particles in 200 mg/l aqueous solution of acetic acid at about 100° C, both catalysts showed poor activity. Apparently, activity is associated with chromium in the +6 valence state, which is water soluble. Palladium (0.1 wt. % on Al_2O_3, G-63D) and CuO·ZnO (G-66B) were inactive. Copper (G-T317) and iron oxide (G-3A) both demonstrated intermediate activities with no signs of early deactivation.

Iron oxide was subjected to further testing to see if reproducible rates could be measured. The following pretreatment procedure gave satisfactory results. Chemetron G-3A catalyst is an unsupported, chromium promoted material. To remove the chromium, the particles were first boiled for 5 hr. in a 200 mg/l acetic acid solution. After it was dried, this material had a surface area of 74.7 sq. m/g (nitrogen adsorption), a solid

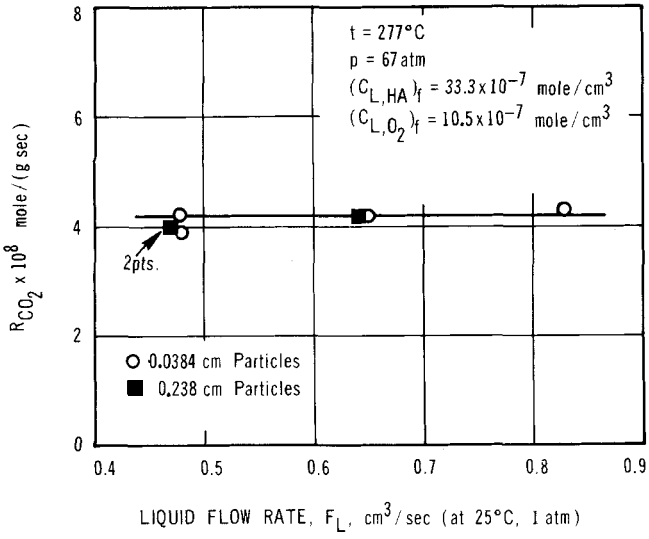

Fig. 2. Effect of liquid flow rate on reaction rate in a differential, liquid full reactor.

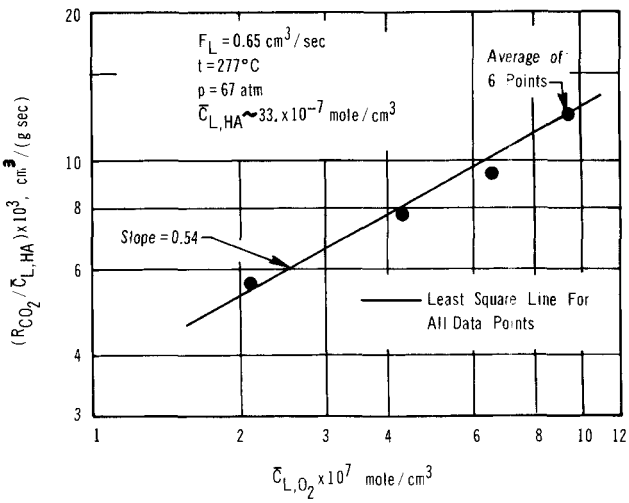

Fig. 3. Effect of oxygen concentration on intrinsic rate.

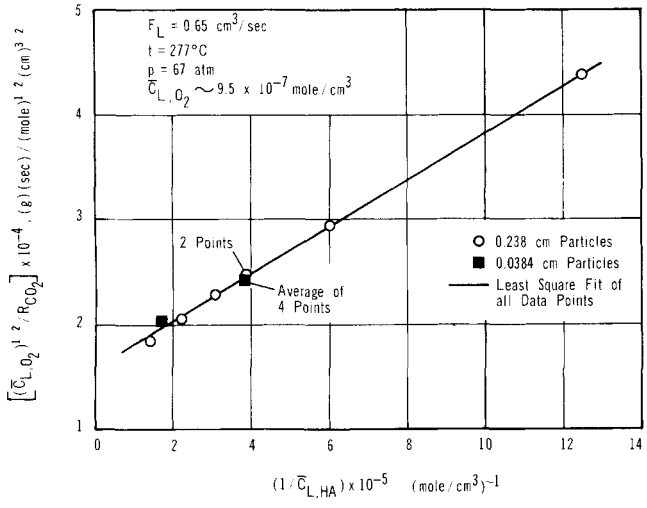

Fig. 4. Effect of acetic acid concentration on rate.

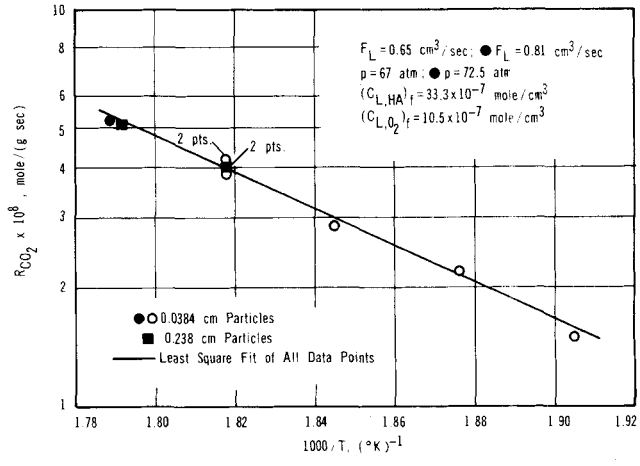

Fig. 5. Effect of temperature and particle size on rate in differential, liquid full reactor.

phase density of 4.14 g/cm³, and particle density of 2.05 g/cm³. The two densities correspond to a porosity of 0.51. To obtain stable activity, the dried catalyst had to be treated in situ for about 10 hr. at 277°C with a liquid feed stream of acetic acid (200 mg/l) in water saturated with pure oxygen (at 1 atm). During this pretreatment, the rate of production of carbon dioxide was less than the stoichiometrically equivalent (for CH_3COOH oxidation) rate of disappearance of oxygen. Further, the catalyst was black when packed in the reactor but reddish after removal. Evidently oxidation to ferric oxide occurs during pretreatment. Such an oxidized form of the catalyst gave reproducible rates of carbon dioxide production for a period of at least 62 hr.

As noted in Table 1, intrinsic kinetics experiments were made with two sizes of catalyst particles: 35 to 42 mesh (average spherical $d_p = 0.0386$ cm) and 3 × 3 mm (⅛ in. × ⅛ in.) cylindrical pellets cut in half which corresponds to $d_p = 0.238$ cm. For trickle-bed experiments, 28 to 32 mesh particles ($d_p = 0.0541$ cm) and the cut pellets $d_p = 0.238$ cm were employed.

INTRINSIC KINETICS

The differential reactor runs in the liquid full reactor were employed to evaluate the accuracy of the analytical methods. Since measurable concentrations of intermediates were not detected, carbon and oxygen mass balances could be formulated in terms of the carbon dioxide, TOC and oxygen analyses of the product stream according to the overall reaction $CH_3COOH + 2O_2 \rightarrow 2CO_2 + 2H_2O$. The carbon in the stripped gas (carbon dioxide analysis) plus the carbon from the TOC analysis of stripped liquid should be equal to the carbon in the CH_3COOH in the feed. Such complete analyses were made for six runs, with deviations ranging from 0 to +5% or −4% of the carbon converted. Oxygen mass balances were less accurate because the difference between oxygen content in the feed and product streams was small. For the same six runs, the deviation between the dissolved oxygen in the feed and the oxygen in the stripped gas from the product varied from 1 to +14% or −7% of the oxygen reacting.

On the basis of these mass balance results, and since the carbon dioxide concentration in the liquid feed was essentially zero, reaction rates were calculated from the carbon dioxide analyses by using the equation

$$R_i = \frac{F_L}{W}\left[(C_i)_e - (C_i)_f\right] \qquad (1)$$

where $C_f = 0$ for carbon dioxide. Rates so calculated for runs at identical conditions were reproducible within 5%. Blank runs with glass beads but no catalyst particles did not show measurable carbon dioxide production. Since the mass balances were satisfactory for the six test runs, only carbon dioxide and oxygen analyses were made for all other runs. The ranges of conversions were 8 to 25% for oxygen and 1 to 5% for acetic acid.

Initially, runs were made for various liquid rates and for both particle sizes at near the highest temperature, 277°C.

The resulting rates, shown in Figure 2, are independent of both of these variables. It was concluded that for these conditions both liquid-to-particle and intraparticle diffusion effects were negligible. Further data were taken at a liquid flow rate of 0.65 cm³/s.

The effect of oxygen on the rate is illustrated in Figure 3 where $R_{CO_2}/\overline{C}_{HA}$ is plotted vs. the arithmetic average oxygen concentration. For these points, the acetic acid concentration did not vary significantly through the reactor since the conversion was of the order of 1%. The data points in Figure 3 suggest that the rate is one-half order in oxygen.

Similar runs for a range of acetic acid concentrations (50 to 500 p.p.m.) show a linear effect at low concentrations but approaching zero order at high C_{HA}. According to these results, the rate equation is of the form

$$R_{CO_2} = -R_{O_2} = -2R_{HA} = \frac{K' C_{HA}}{1 + K'' C_{HA}} C_{O_2}^{1/2} \quad (2)$$

The linearized version of Equation (2) is plotted in Figure 4 along with the data points for different acetic acid concentrations. Data for both particle sizes agree with Equation (2).

Figure 5 is an Arrhenius plot of rate data for the two catalyst particle sizes taken at different temperatures and at constant feed composition. The agreement between the rates for the two particle sizes confirms the absence of intraparticle and liquid-to-particle diffusion effects. These data were analyzed by writing Equation (2) in the form

$$\frac{R_{CO_2}}{C_{O_2}^{1/2}} = \frac{A' [\exp(-E'/RT)] C_{HA}}{1 + A'' [\exp(-E''/RT)] C_{HA}} \quad (3)$$

Regression analysis (least square) indicated that E'' was nearly zero and $E' = 21$ kcal/mole. The values of A' and A'' (or K'') are shown in the following final equation for the rate:

$$R_{CO_2} = \frac{9.9 \times 10^9 \exp(-21\,000/RT)\, C_{HA}\, C_{O_2}^{1/2}}{1 + 7.2 \times 10^5\, (C_{HA})} \quad (4)$$

This numerical expression was used for the intrinsic rate in the subsequent calculations for trickle-bed reactor operation.

The mechanism of the oxidation cannot be determined from our data. However, with the help of other information for organic acid oxidations, it can be shown that the form of Equation (2) is not illogical, provided that the oxidation is wholly heterogeneous. The pretreatment experiments of Goto and Smith (1974*b*) with formic acid and those here with acetic acid indicate that catalyst activity is associated with an oxidized state. Hence, it is likely that the acid first reacts with an oxidized site on the catalyst surface, ultimately forming carbon dioxide and water via multiple steps, and that the reduced site is reoxidized by adsorption of oxygen. While we found no measurable concentrations of intermediates, they could exist on the catalyst at small concentrations, though their individual lifetimes may be short. Gorshkov et al. (1968) and Margolis (1971) supposed, for acetaldehyde oxidation, that these intermediates were formaldehyde-carbon monoxide- and formic acid-types of species. If it is assumed that similar intermediates or free radicals are formed in the liquid phase oxidation of acetic acid, though not necessarily HCHO, HCOOH, and CO, and that these adsorbed intermediates may be denoted as [HCHO], [CO], and [HCOOH], the mechanism may be written in terms of the following elementary steps:

$$CH_3COOH + X \underset{k_1'}{\overset{k_1}{\rightleftarrows}} CH_3COOH \cdot X \quad (5)$$

$$\tfrac{1}{2}O_2 + X \underset{k_2'}{\overset{k_2}{\rightleftarrows}} O \cdot X \quad (6)$$

$$CH_3COOH \cdot X + O \cdot X \xrightarrow{k_3} [HCHO] + [CO] + H_2O + X \quad (7)$$

$$[HCHO] + O \cdot X \xrightarrow{k_4} [HCOOH] + X \quad (8)$$

$$[HCOOH] + O \cdot X \xrightarrow{k_5} CO_2 + H_2O + X \quad (9)$$

$$[CO] + O \cdot X \xrightarrow{k_6} CO_2 + X \quad (10)$$

where X indicates a vacant site and $O \cdot X$ an oxidized site capable of acting as a catalyst for reaction (7). Combination of Equations (5) to (10) leads to the overall reaction mentioned earlier. Since the concentrations of oxygen and acetic acid are very low, the fraction of the sites occupied will be low so that the concentration C_x of vacant sites may be regarded as constant, independent of concentrations of adsorbed species. Equations (5) and (6) represent reversible adsorption of CH_3COOH and oxygen, while Equation (7) is slow and supposed to control the rate. The intermediates decomposition reactions are assumed to be fast so that the stationary state assumption is valid for [HCHO], [CO], and [HCOOH] as well as for adsorbed $CH_3COOH \cdot X$ and $O \cdot X$. This permits expressing the concentrations of $O \cdot X$, [HCOOH], [CO], and [HCHO] in terms of acetic acid C_{HA} and oxygen concentrations. If it is further assumed that $k_2' >> k_3$, the concentration of $O \cdot X$, for example, may be written

$$C_{O \cdot X} = \frac{K_{O_2} C_x C_{O_2}^{1/2}}{1 + \left[4 C_x \frac{k_3}{k_2} K_{O_2} K_{HA}\right] C_{HA}} \quad (11)$$

The rate of production of carbon dioxide is given by Equations (9) and (10):

$$R_{CO_2} = k_5 C_{[HCOOH]} C_{O \cdot X} + k_6 C_{[CO]} C_{O \cdot X} \quad (12)$$

Substituting Equation (11) and similar expressions for $C_{[HCOOH]}$ and $C_{[CO]}$ into (12), we get the final expression for the rate:

$$R_{CO_2} = \frac{(2k_3 C_x^2 K_{O_2} K_{HA})\, C_{HA}\, C_{O_2}^{1/2}}{1 + \left[4\left(\frac{k_3}{k_2}\right) C_x K_{O_2} K_{HA}\right] C_{HA}} \quad (13)$$

where K_{HA} and K_{O_2} are adsorption equilibrium constants equal to k_1/k_1' and k_2/k_2', respectively. Equation (13) is of the same form as Equation (2).

Equation (4) gives rates several orders of magnitude lower, at the same temperature, than R_{CO_2} for the oxidation of formic acid determined by Baldi et al. (1974). The activation energy was 37 kcal/mole for formic acid vs. 21 kcal/mole shown by Figure 5. Also, different concentration dependences were observed. The slow step involving the destruction of the CH_3 group, that is, Equation (7), is not involved with formic acid.

TRICKLE-BED OPERATION

For the trickle bed, global rate measurements small amounts of catalyst were employed so that conversions were from 10 to 20% for acetic acid and 2 to 5% for oxygen. Since equilibrium was closely approached in the second separator, R_{CO_2} was obtained from the measured

Table 2. Physical Properties and Oxygen Solubility at 67 atm

t, °C	ρ[a], g/cm³	μ[b] × 10³, g/(cm) s	$D^c_{O_2}$ × 10⁴, cm²/s	D^c_{HA} × 10⁴, cm²/s	(H'_{O_2})[d] × 10⁻⁴, atm	H_{O_2}, cm³/cm³
252	0.808	1.178	2.104	1.213	2.565	0.89
260	0.801	1.153	2.154	1.242	2.362	1.05
269	0.780	1.080	2.314	1.334	2.141	1.49
277	0.768	1.045	2.399	1.384	1.951	2.87
286*	0.759*	1.017*	2.472*	1.425*	1.766*	4.05*

* At 72.5 atm.
[a] Lydersen, Greenkorn, and Hougen method; Reid and Sherwood (1966).
[b] Stiel and Thodos method; Jossi et al. (1962).
[c] Othmer-Thakar equation; Reid and Sherwood (1966).
[d] Himmelblau (1960), based upon $P_{O_2} = H'_{O_2} x_{O_2}$, where x is the mole fraction of oxygen in the liquid and P_{O_2} = partial pressure of oxygen in gas.

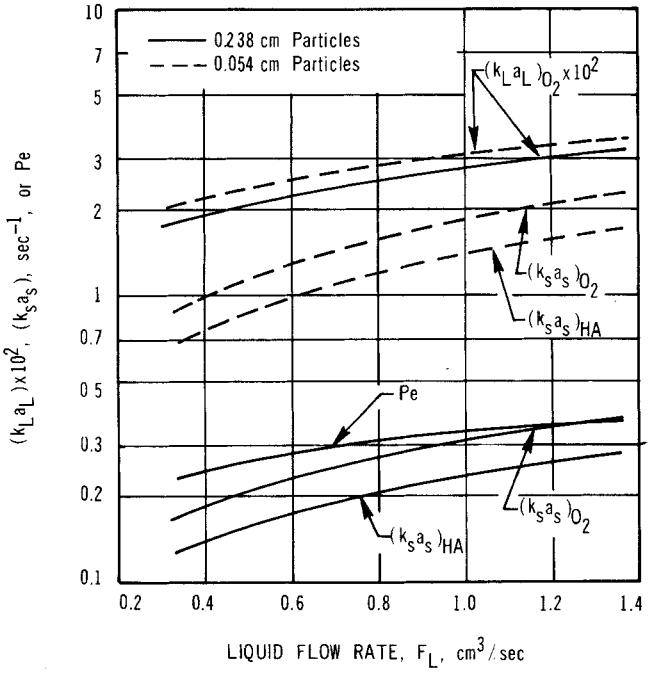

Fig. 6. Predicted mass transfer coefficients at 277°C and 67 atm.

flow rates and liquid composition according to the equation

$$R_{CO_2} = \frac{(F_L + H_{CO_2} F_g)(C_{L,CO_2})_e - F_L(C_{L,CO_2})_f}{W} \qquad (14)$$

where H_{CO_2} is Henry's law constant and has a value of 1.20 [g mole/(cm³ of gas)]/[g mole/(cm³ of liquid)], both volumes at 25°C and 1 atm. pressure. Note that both F_L and F_g were measured at 25°C and 1 atm. pressure. Global rates were obtained as a function of gas and liquid flow rates, temperature, and catalyst particle size (see Table 1 for range of operating conditions).

For integral reactor runs, experimental conversions were obtained as a function of liquid flow rate and ranged from 42 to 77.5%. Data were taken for but one particle size (d_p = 0.238 cm) and at 277°C. The conversion was calculated from TOC analysis of the reactor effluent. The feed consisted of a liquid stream containing 200 p.p.m. of acetic acid, saturated with air at 1 atm pressure, and a gas stream of high pressure air (Figure 1).

Auxiliary Information

To predict global rates and integral-reactor conversions, mass transfer coefficients from gas-liquid interface to bulk liquid (k_La_L) and from bulk liquid to particle surface (k_sa_s) are required, both at operating temperature and pressure. For a slightly soluble gas like oxygen, it is satisfactory to assume that the gas-liquid interface concentration is the equilibrium value corresponding to bulk gas concentration. However, the solubility, or Henry's law constant H_{O_2}, is needed. Goto and Smith (1975*a*) measured $(ka)_L$ and $(ka)_s$ at atmospheric pressure and room temperature for the particle size range and flow rates used here and also summarized the meager data available in the literature. In the absence of experimental results at high pressures and temperatures, we will use their dimensional correlations, which are

$$\frac{(k_La_L)}{D} = \alpha_L \left(\frac{G_L}{\mu}\right)^{n_L} \left(\frac{\mu}{\rho D}\right)^{1/2} \qquad (15)$$

and

$$\frac{(k_sa_s)}{D} = \alpha_s \left(\frac{G_L}{\mu}\right)^{n_s} \left(\frac{\mu}{\rho D}\right)^{1/3} \qquad (16)$$

where $\alpha_L = 7.8$, $n_L = 0.39$, $\alpha_s = 153$, and $n_s = 0.67$ for $d_p = 0.0541$ cm, and $\alpha_L = 6.3$, $n_L = 0.41$, $\alpha_s = 45$, and $n_s = 0.56$ for $d_p = 0.238$ cm. To use these correlations for predicting coefficients at 67 atm and 252° to 286°C, densities and viscosities of water and diffusivities of acetic acid and oxygen have to be known at these conditions. Since experimental data are unavailable for the most part, such properties were estimated by using the methods listed in the footnotes to Table 2. These procedures were considered to be most accurate at present, although some error may result, particularly for diffusivities and in assuming that α and n in Equations (15) and (16) are independent of temperature and pressure. Table 2 also includes experimental values obtained by Himmelblau (1960) for Henry's law constant for oxygen. The coefficients calculated from Equations (15) and (16) by using these property values (Table 2) are shown in Figure 6 for 277°C and for 0.0541 and 0.238 cm catalyst particles. Results were similar for other temperatures.

If axial dispersion in the liquid is considered in the model for trickle-bed performance, an axial Peclet number Pe is needed. In the absence of experimental data, Pe was estimated from the correlation of Furzer and Michell (1970). This correlation, which was based primarily on counterflow of gas and liquid, involves the dynamic holdup H_d; that is

$$Pe = \frac{d_p u_L}{E} = 4.3 \left(\frac{Re}{H_d}\right)^{1/2} (Ga)^{-1/3} \qquad (17)$$

The dynamic holdup was obtained from the dimensional equation of Satterfield and Way (1972):

$$H_d = A(u_L)^{1/3} (100\,\mu)^{1/4} \qquad (18)$$

Goto and Smith (1975*a*) determined A to be 0.483 (cm/s)$^{-1/3}$ [g/(cm s)]$^{-1/4}$ for granular particles of about the same size ($d_p \sim 0.238$ cm) as used here. Equations (17)

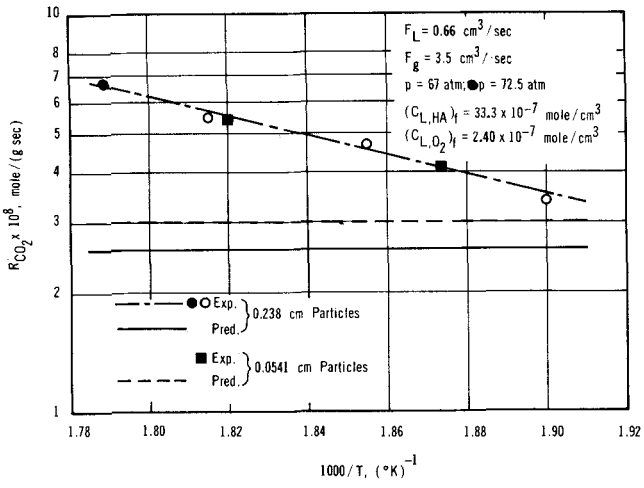

Fig. 7. Effect of temperature on global rate (differential, trickle-bed reactor results).

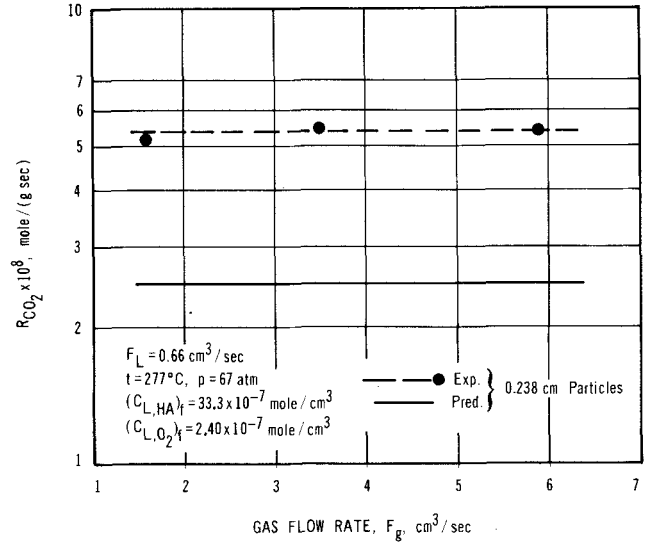

Fig. 8. Effect of F_g on global rate in differential, trickle-bed reactor.

and (18) with $A = 0.483$ were used to account for axial dispersion in the integral reactor model to predict conversions. The Pe numbers at 277°C are also shown in Figure 6.

Differential Reactor Results

Experimentally determined [Equation (14)] global rates are shown by the data points in Figures 7 to 9. No effect of F_g was observed, but R_{CO_2} increased with liquid rate (Figure 9) in agreement with the results of Goto and Smith (1975*a*) who found that k_La_L and k_sa_s were independent of F_g but increased with F_L. Figure 7 shows the temperature effect, and it is noted that the data points establish a line with a lower slope than that obtained for the intrinsic rate (Figure 5). This difference is not due solely to external diffusional resistances retarding the trickle-bed results but also to the decrease in partial pressure of oxygen in the gas as the temperature is increased. As T increases, the vapor pressure of water rises so that at constant total pressure the partial pressure of oxygen must decrease. This reduces C^*_{L,O_2} and the rate of reaction. The increase in R_{CO_2} with liquid flow rate shown in Figure 9 represents the decreasing importance of mass transfer resistances and reflects the small increase in (k_La_L) and (k_sa_s) with F_L shown in Figure 6. The data points in Figures 7 and 9 show no effect of particle size, verifying the conclusion from intrinsic rate experiments that intraparticle diffusion does not retard the rate. Also, for this system k_La_L is much smaller than k_sa_s (Figure 6) so that

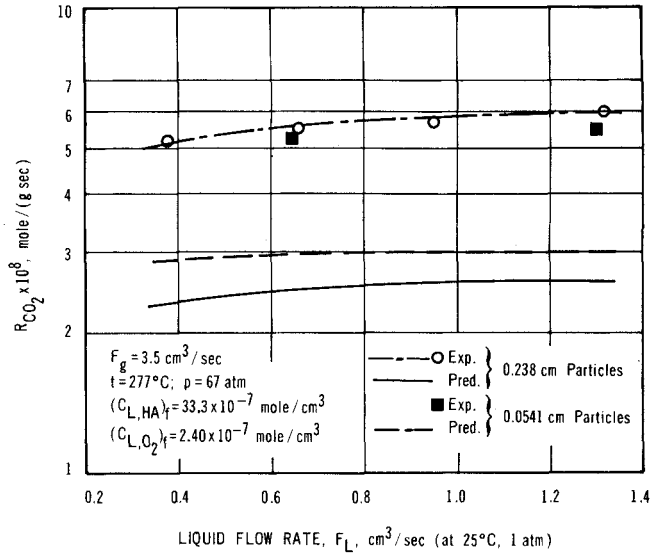

Fig. 9. Effect of F_L on global rate in differential, trickle-bed reactor.

k_La_L is the major external transport resistance. As Figure 6 shows, k_La_L changes but little with particle size, indicating that external diffusion resistance, even though it is significant, is not strongly affected by d_p. This also is part of the explanation of why the rates in Figures 8 and 9 are not affected by particle size.

For comparison, global rates were calculated from intrinsic kinetics [Equation (4)], and (k_La_L) and (k_sa_s) by employing the following model: oxygen is transferred from gas to bulk liquid (rate coefficient k_La_L), both oxygen and acetic acid are transferred from liquid to particle surface (rate coefficient k_sa_s), and reaction within the catalyst particle occurs at surface concentrations, C_{s,O_2}, $C_{s,HA}$. It is assumed that the concentration profiles across the gas interface-bulk liquid and liquid-particle surface do not overlap. Then mass balances over the whole differential reactor may be written as

$$F_L[(C_{L,O_2})_e - (C_{L,O_2})_f] = 2F_L[\overline{C}_{L,O_2} - (C_{L,O_2})_f]$$
$$= (k_La_L)_{O_2} S z_B (C^*_{L,O_2} - \overline{C}_{L,O_2})$$
$$- (k_sa_s)_{O_2} S z_B (\overline{C}_{L,O_2} - \overline{C}_{s,O_2}) \quad (19)$$

$$F_L[(C_{L,HA})_f - (C_{L,HA})_e] = 2F_L[(C_{L,HA})_f - \overline{C}_{L,HA}]$$
$$= (k_sa_s)_{HA} S z_B (\overline{C}_{L,HA} - \overline{C}_{s,HA}) \quad (20)$$

where the overbar represents arithmetic average values at the feed (f) and exit (e) ends of the reactor. The bulk concentrations C_{L,O_2}, $C_{L,HA}$ are related to the surface values by the following equations applicable at the outer surface of the particles:

$$\frac{1}{\rho_B}(k_sa_s)_{O_2}(\overline{C}_{L,O_2} - \overline{C}_{s,O_2}) = \frac{K'\overline{C}_{s,HA}}{1 + K''C_{s,HA}}(\overline{C}_{s,O_2})^{1/2} \quad (21)$$

$$\frac{1}{\rho_B}(k_sa_s)_{HA}(\overline{C}_{L,HA} - \overline{C}_{s,HA})$$
$$= \frac{1}{2}\frac{K'\overline{C}_{s,HA}}{1 + K''C_{s,HA}}(\overline{C}_{s,O_2})^{1/2} \quad (22)$$

Equations (19) to (22) can be solved by trial for the four unknowns $\overline{C}_{L,O_2}$, $\overline{C}_{L,HA}$, $\overline{C}_{s,O_2}$, $\overline{C}_{s,HA}$ and then the surface values used in Equation (4) to obtain a predicted rate. Such predicted values are shown by the solid and dashed lines in Figure 7 as a function of temperature at constant flow rates. Agreement is relatively good at the lowest tem-

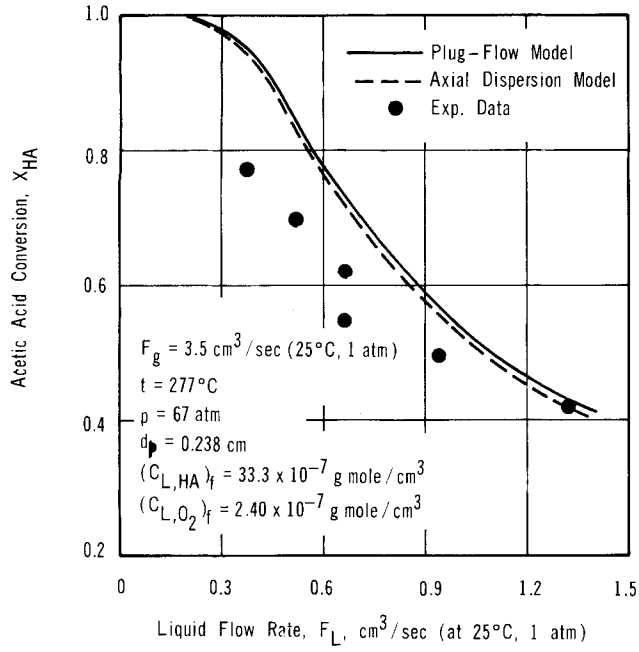

Fig. 10. Effect of liquid flow rate on conversion of acetic acid in integral, trickle-bed reactor.

peratures, but experimental rates are much higher at higher temperatures. This suggests that the model and mass transport coefficients are reasonably satisfactory at the lower temperatures. Uncertainties exist in (k_La_L) and in (k_sa_s) because of estimated molecular diffusivities and errors in the correlations, Equations (15) and (16). Such uncertainties may explain the small deviation at the lowest temperature. Since (k_La_L) is much less than (k_sa_s) (Figure 6), only uncertainties in (k_La_L) would be significant. Since concentrations are very low, the maximum temperature rise due to the exothermic reaction is less than 0.1°C. Hence, an intraparticle temperature rise does not seem to be a reasonable explanation for the high rates.

The model presumes that no gas comes into contact directly with the particles. Direct contact could eliminate much of the retardation due to k_La_L and k_sa_s and substitute the resistance due to a very thin film of liquid around the particle. Hartman and Coughlin (1972) in integral reactor studies introduced a factor to account for direct gas contacting in order to obtain agreement between experimental and predicted conversions. At the higher temperatures of our study, the vapor pressure of water (60.4 atm at 277°C) is close to the total pressure (67 atm). Hence, local regions on the particle surface might periodically be exposed to gas rather than liquid with resulting higher rates of reaction. This could explain the increase in experimental rate with temperature.

The predicted rates in Figure 7 change little with temperature. The increase in intrinsic rate with temperature increase is balanced by the decrease due to the drop in oxygen pressure in the gas. Again, this is caused by the sharp increase in water vapor pressure with temperature, in the temperature range studied. A small amount of water must vaporize upon entering the reactor from the distributor, but apparently this was insufficient to cause a significant drop in temperature in the reactor. Thermocouple readings in the water feed, top, and bottom of the reactor were all within 2°C.

In the formic acid studies (Goto and Smith, 1975*b*) relatively good agreement between experimental and predicted rates was obtained over the entire temperature range, 212° to 240°C. However, at these lower temperatures, the vapor pressure of water increased more slowly with temperature so that the vaporization phenomena may not have occurred. The predicted rates in the case of formic acid increased with temperature, in contrast to those shown in Figure 7 for acetic acid. This was due not only to the smaller increase in water vapor pressure but also to the larger activation energy for formic acid, 37 vs. 21 kcal/mole.

The effect of flow rates on R_{CO_2} was measured only at a relatively high temperature, 277°C. This is why the predicted results deviate greatly from the experimental values in Figures 8 and 9. Predicted and experimental rates show the same trend with flow rates.

The deviations evident in Figures 7 to 9 indicate that more research is needed in trickle beds at temperatures near the boiling point of the liquid phase.

Integral Reactor Results

The experimental conversions of acetic acid were calculated from compositions by using the equation

$$X_{HA} = \frac{(C_{L,HA})_f - (C_{L,HA})_e}{(C_{L,HA})_f} \tag{23}$$

Conversions of oxygen (32 to 62%) were calculated in a similar manner by using the gas analysis from the stripping column. Figure 10 shows the effect of liquid flow rate on X_{HA} at 277°C. Measurements were not made at other temperatures.

Conversions were predicted by using the same mass transfer model and assumptions that were employed to predict global rates plus the following assumptions about the behavior of the reactor as a whole.

1. Axial dispersion in the gas phase is negligible.
2. Radial gradients of concentration and velocities are negligible.
3. Gas and liquid flow rates do not vary in the axial direction.

With this reactor model, the mass balances and boundary conditions are:

oxygen in gas phase

$$F_g \frac{d\,C_{g,O_2}}{dz} + (k_La_L)_{O_2}\, S(C^*_{L,O_2} - C_{L,O_2}) = 0 \tag{24}$$

oxygen in liquid phase

$$E\,S \frac{d^2\,C_{L,O_2}}{dz^2} - F_L \frac{d\,C_{L,O_2}}{dz} + (k_La_L)_{O_2}\, S(C^*_{L,O_2} - C_{L,O_2}) - (k_sa_s)_{O_2}\, S(C_{L,O_2} - C_{s,O_2}) = 0 \tag{25}$$

acetic acid in liquid phase

$$E\,S \frac{d^2\,C_{L,HA}}{dz^2} - F_L \frac{d\,C_{L,HA}}{dz} - (k_sa_s)_{HA}\, S(C_{L,HA} - C_{s,HA}) = 0 \tag{26}$$

The axial dispersion coefficient E was obtained from Equation (17). By including axial dispersion in the liquid phase, the solution of Equations (24) to (26) for the concentration profiles becomes a two-point boundary value problem according to the following conditions:

at $z = 0$

$$C_{g,O_2} = (C_{g,O_2})_f \tag{27}$$

$$-E\,S \frac{d\,C_{L,O_2}}{dz} = F_L[(C_{L,O_2})_f - C_{L,O_2}] \tag{28}$$

$$-E\,S \frac{d\,C_{L,HA}}{dz} - F_L[(C_{L,HA})_f - C_{L,HA}] \tag{29}$$

at $z = z_B$

$$\frac{d\,C_{L,O_2}}{dz} = 0 \tag{30}$$

$$\frac{dC_{L,HA}}{dz} = 0 \qquad (31)$$

The equilibrium oxygen concentration in the liquid is related to the gas concentration by Henry's law $C^*_{L,O_2} = C_{g,O_2}/H_{O_2}$. For water saturated with air at 277°C and 67 atm, the data in Table 2 for H'_{O_2} give

$H_{O_2} = 2.87$[mole/(cm³ of air at 25° cm, 1 atm)]/

[mole/(cm³ of liquid at 277°C, 67 atm)]

Equations (24) to (31) with (21) and (22) can be solved numerically to determine concentration profiles for oxygen and acetic acid in the liquid phase and oxygen in the gas phase. The solution procedure was initiated by assuming values for C_{g,O_2}, C_{L,O_2}, and $C_{L,HA}$ at $z = z_B$ and then by integrating Equations (24) to (26) back to $z = 0$ with boundary conditions given by Equations (30) and (31). The stepwise HPCG method (Hemmings Predictor-Corrector Method, IBM Manual, 1970) was used for the integration. If the calculated concentrations at $z = 0$ satisfied Equations (27) to (29), the assumed values at $z = z_B$ were correct.

If axial dispersion in the liquid is neglected (plug flow model), the terms involving the second derivative in Equations (25) and (26) disappear and only the boundary conditions at $z = 0$ corresponding to the feed composition are needed. Predicted acetic acid conversions by both axial dispersion and plug flow models are also shown in Figure 10, and predicted concentration profiles are given in Figure 11.

Except at the highest flow rate, the experimental conversions in Figure 10 are considerably lower than predicted values. Such deviations are in the opposite direction from the differences between global rates shown in Figure 9. Low conversions could be caused by channeling of the liquid so that part of the catalyst is not exposed to acetic acid. Catalyst bed depth for the integral runs was eight times as large as for the differential runs (Table 1). Hence, channeling may have been unimportant in the latter runs, while in the integral reactor liquid could have migrated toward the reactor wall as the bed depth increased. This effect would probably be more important at low liquid rates and could explain the much larger deviations between experimental and predicted conversions at low F_L. In the formic acid study, experimental conversions were also lower than predicted values, at the lowest flow rates, but the difference was less than in Figure 10. This probably was because high conversions could be obtained for formic acid with shorter bed depths and higher liquid rates.

The curves in Figure 10 for the two models suggest that axial dispersion did not have a large effect on conversion and could not explain the difference between experimental and predicted conversions.

The predicted concentration profile for oxygen in the liquid, illustrated in Figure 11, increases strongly near the entrance to the reactor. This reflects the fact that the intrinsic reaction rate is too low to utilize all the oxygen transferred from gas to liquid. For the oxidation of formic acid (Goto and Smith, 1975*b*), the intrinsic rate was much higher and the concentration profile was of the reverse shape, mildly concave upwards. Figure 11 also shows that the difference between bulk-liquid and particle-surface concentrations was small. This is expected from the curves in Figure 6, indicating that $(k_s a_s)$ is one order of magnitude greater than $(k_L a_L)$. On the other hand, $(k_L a_L)$ significantly affects the overall results. Figure 12 gives predicted concentration profiles computed for $k_L a_L = \infty$, for comparison with predicted profiles based upon the presumably correct

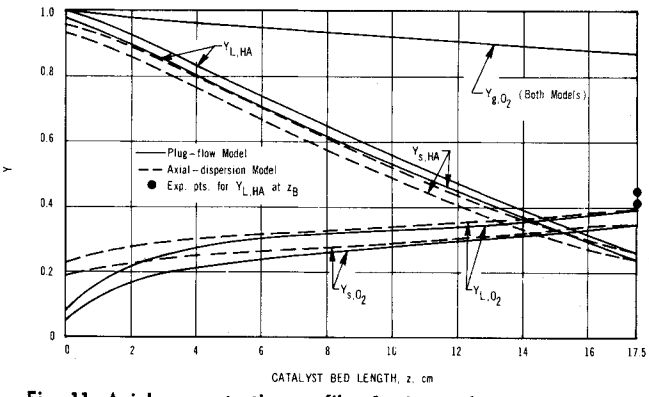

Fig. 11. Axial concentration profiles for integral, trickle-bed reactor (d_p = 0.238 cm, F_g = 3.5 cm³/s; F_L = 0.66 cm³/s; t = 277°C; p = 67 atm).

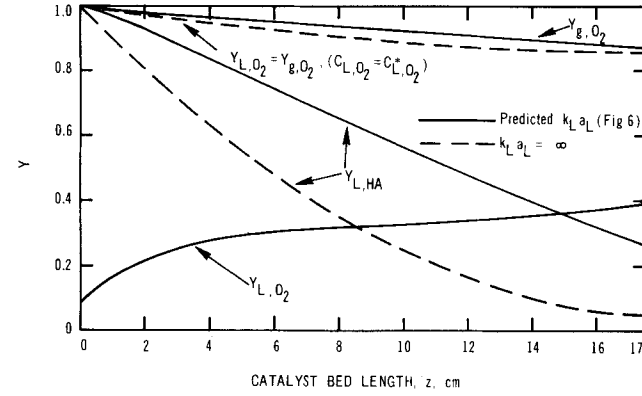

Fig. 12. Effect of gas-liquid mass transport (plug flow model) (d_p = 0.238 cm, F_g = 3.5 cm³/s; F_L = 0.66 cm³/s; t = 277°C, p = 67 atm).

$k_L a_L$ values in Figure 6. The difference indicates that mass transfer resistance from gas to liquid has a strong affect even for this relatively slow reaction. For example, even at the entrance to the bed, if $(k_L a_L) = \infty$, $(C_{L,O_2})_f = (C^*_{L,O_2})_f$ and $Y_{L,O_2} = 1.0$. Thus, the Y_{L,O_2} curves in Figure 12 for finite and infinite $(k_L a_L)$ differ greatly.

These quantitative comparisons between predicted and experimental global rates and conversions suggest that more research is needed on trickle-bed operation. In particular, more complete studies are needed with liquids near their boiling point in order to evaluate the effect of direct contact of gas with catalyst particle, and more information is needed about the effect of liquid channeling as a function of catalyst bed depth and liquid flow rate. Also, it would be helpful to have experimental verification at elevated pressures and temperatures of the correlations for mass transfer coefficients.

ACKNOWLEDGMENT

The fellowship aid of the International Research and Exchanges Board is gratefully acknowledged. We also thank the Chemetron Corporation for the many samples of catalysts used in this study.

NOTATION

A = parameter in Equation (18), $(\text{cm/s})^{-1/3}$ $[\text{g/(cm s)}]^{-1/4}$

A' = preexponential factor in Equation (3), $(\text{cm})^{4.5}/[(\text{mole})^{1/2}\ (\text{g s})]$

A'' = constant in Equation (3), cm³/mole

a = effective mass transfer, cm²/(cm³ of empty reactor); a_L = gas-to-liquid area, a_s = liquid-to-particle area

C = concentration, mole/cm³

C_L^* = concentration in liquid in equilibrium with gas, mole/cm³
$\overline{C}$ = arithmetic average concentration, mole/cm³
C_x = concentration of active sites on catalysts, number of sites/(g of catalyst)
D = molecular diffusivity in liquid, cm²/s
d_p = equivalent spherical, particle diameter, cm
E = axial dispersion coefficient, cm²/s
E' = activation energy, Equation (3), kcal/mole
E'' = constant in Equation (3), kcal/mole
F_g = volumetric flow rate of gas at 25°C, 1 atm, cm³/s
F_L = volumetric flow rate of liquid at reactor temperature and pressure, except where noted, cm³/s
G_a = Gallileo number, $d_p^3\ g\ \rho^2/\mu^2$
G_L = superficial mass velocity of liquid, g/(cm² s)
g = acceleration of gravity, cm/s²
H' = Henry's law constant, atm; defined as $P_i = H'x_i$ where x_i = liquid phase mole fraction of component i at partial pressure P_i
H_{O_2} = Henry's law constant (cm³ of liquid at temperature and pressure)/(cm³ of gas at 25°C and 1 atm), $C_g = HC_L^*$
H_d = dynamic holdup, (cm³ of liquid)/(cm³ of empty reactor)
K' = constant in Equation (2), $(\text{cm})^{4.5}/[(\text{mole})^{0.5}\ (\text{g s})]$
K'' = constant in Equation (2), cm³/mole
K_{HA} = adsorption equilibrium constant for acetic acid
K_{O_2} = adsorption equilibrium constant for oxygen
k_L = mass transfer coefficient from gas-liquid interface to liquid, cm/s
k_s = mass transfer coefficient from liquid to particle surface, cm/s
n_L = parameter in Equation (15)
n_s = parameter in Equation (16)
Pe = axial Peclet number, $d_p\ u_L/E$
R = reaction rate, mole/(g s)
Re = Reynolds number, $d_p\ G_L/\mu$
S = cross-sectional area of reactor, cm²
T = temperature, °K
t = temperature, °C
u_L = superficial velocity of liquid, cm/s
W = mass of catalyst, g
X = active catalyst site
X_{HA} = conversion of acetic acid in liquid at the exit of the reactor
$Y_{g,O_2} = C_{g,O_2}/(C_{g,O_2})_f$
$Y_{L,O_2} = C_{L,O_2}/(C^*_{L,O_2})_f$
$Y_{s,O_2} = C_{s,O_2}/(C^*_{L,O_2})_f$
$Y_{L,HA} = C_{L,HA}/(C_{L,HA})_f$
$Y_{s,HA} = C_{s,HA}/(C_{s,HA})_f$
z = axial coordinate in reactor, cm
z_B = total length of catalyst bed, cm
α_L = parameter in Equation (15), $(\text{cm})^{n_L-2}$
α_s = parameter in Equation (16), $(\text{cm})^{n_s-2}$
ρ_B = bulk density of catalyst bed, g/cm³ of reactor filled with catalyst particles
μ = fluid viscosity, g/(cm s)

Subscripts

HA = acetic acid
e = exit
f = feed
g = gas phase
i = component i
L = liquid phase
s = particle surface

LITERATURE CITED

Baldi, G., S. Goto, C. K. Chow, and J. M. Smith, "Catalytic Oxidation of Formic Acid in Water," *Ind. Eng. Chem. Process Design Develop.*, **13**, 447 (1974).

Furzer, I. A., and R. W. Michell, "Liquid-Phase Dispersion in Packed Beds with Two Flow," *AIChE J.*, **16**, 380 (1970).

Gorshkov, A. P., I. K. Kolchin, A. M. Gribov, and L. Ya. Margolis, "Conversion of the Oxygen-Containing Products of Propylene Oxidation on Bismuth Molybdate," *Kinetika i Kataliz*, **9**, 1086 (1968).

Goto, Shiego, and J. M. Smith, "Trickle-Bed Reactor Performance. Part I. Holdup and Mass Transfer Effects," *AIChE J.*, **21**, 706 (1975*a*).

———, "Trickle-Bed Reactor Performance. Part II. Reaction Studies," *ibid.*, 714 (1975*b*).

Hamilton, C. E., J. L. Teal, and J. A. Kelley, *U.S. Patent No. 3.442.802* (May 6, 1969).

Hartman, M., and R. W. Coughlin, "Oxidation of SO_2 in a Trickle-Bed Reactor Packed with Carbon," *Chem. Eng. Sci.*, **27**, 867 (1972).

Himmelblau, D. M., "Solubilities of Inert Gases in Water," *J. Chem. Eng. Data*, **5**, 10 (1960).

Jossi, J. A., L. I. Stiel, and George Thodos, "The Viscosity of Pure Substances in the Dense Gaseous and Liquid Phases," *AIChE J.*, **8**, 59 (1962).

Margolis, L. Ya., "On the Mechanism of Catalytic Oxidation of Hydrocarbons," *J. Catalysis*, **21**, 93 (1971).

Programmer's Manual, 5 ed., pp. 337-341, IBM Corp., White Plains, N. Y. (Aug., 1970).

Reid, R. C., and T. K. Sherwood, *The Properties of Gases and Liquids*, 2 ed., McGraw-Hill, New York (1966).

Sadana, A., and J. R. Katzer, "Catalytic Oxidation of Phenol in Aqueous Solution over Copper Oxide," *Ind. Eng. Chem. Fundamentals*, **13**, 127 (1974).

Satterfield, C. N., "Trickle-Bed Reactors," *AIChE J.*, **21**, 209 (1975).

———, and P. F. Way, "The Role of Liquid Phase in the Performance of a Trickle-Bed Reactor," *ibid.*, **18**, 305 (1972).

Sedricks, W., and C. N. Kenney, "Partial Wetting in Trickle-Bed Reactors—The Reduction of Crotonaldehyde over a Palladium Catalyst," *Chem. Eng. Sci.*, **28**, 559 (1973).

Manuscript received August 12, 1975; revision received and accepted October 31, 1975.

Convective Instabilities in Porous Media with Through Flow

The stability of a thermally stratified, saturated porous media through which mass is being ejected is considered theoretically. The stability parameter is a flow modified D'Arcy-Rayleigh number and is a function of a single scalar variable, the dimensionless through-flow strength. Results of both linear and energy theory are given, and it is seen that the fluid can lose stability by either a buoyantly driven mode or by a continuous analogue of the Saffman-Taylor mode.

GEORGE M. HOMSY
Department of Chemical Engineering
Stanford University
Stanford, California 94305

and

ALBERT E. SHERWOOD
Lawrence Livermore Laboratory,
University of California
Livermore, California 94550